

# Band offsets of lattice-matched semiconductor heterojunctions through hybrid functionals and $G_0W_0$

Karim Steiner, Wei Chen,<sup>\*</sup> and Alfredo Pasquarello

*Chaire de Simulation à l'Echelle Atomique (CSEA), Ecole Polytechnique Fédérale de Lausanne (EPFL), CH-1015 Lausanne, Switzerland*

(Received 3 February 2014; revised manuscript received 2 May 2014; published 15 May 2014)

To assess the accuracy of hybrid functional and many-body  $GW$  methods, we study the band offsets for a set of lattice-matched semiconductor heterojunctions, including AlAs/GaAs(100), AlP/GaP(100), Si/GaP(110), Ge/GaAs(110), Ge/AlAs(110), Ge/ZnSe(110), and ZnSe/GaAs(110). The band-edge positions are first obtained for the bulk semiconductors and then aligned through the lineup of a local reference potential at the interface. The band-edge positions critically depend on the electronic-structure method, while the interface dipole is already well accounted for with semilocal density functionals. The two advanced electronic-structure schemes yield consistent valence-band offsets in close agreement with experiment, slightly improving upon semilocal functionals. At variance, conduction-band offsets are subject to larger deviations and improve with the accuracy of the calculated band gaps. In case one is willing to take band gaps from experiment, the best description of the band alignment for the present heterojunctions is achieved by relying on the calculated valence band offsets rather than on hybrid functionals in which the exchange mixing parameter is adjusted.

DOI: [10.1103/PhysRevB.89.205309](https://doi.org/10.1103/PhysRevB.89.205309)

PACS number(s): 73.40.-c, 31.15.E-, 71.15.-m

## I. INTRODUCTION

Heterostructures formed by two semiconductors with almost identical lattice constants but different band gaps, known as lattice-matched semiconductor heterojunctions, are the building blocks of modern electronic and optoelectronic devices, such as light-emitting diodes and field-effect transistors. The difference between the band gaps of the two materials gives rise to a discontinuity of the energy levels at the interface of the heterojunction. This discontinuity, or *band offset*, regulates the carrier injection and transport properties and is the key element for engineering the performance of a heterojunction [1].

For decades, a number of theories have been put forward to help understand and further predict the band offsets of semiconductor heterojunctions [2–14]. Early theoretical attempts rely on the existence of an absolute energy scale derived solely from the bulk material (e.g., as referred to the vacuum level [2,3] or to a neutrality level of the semiconductor [4,9]). These schemes work well in some cases, but without considering the charge dipole at the interface the general accuracy of these methods is in question. The advance of density functional theory (DFT) in the late 1970s enables a self-consistent description of the interface dipole. DFT has been widely applied to various III-V and II-VI semiconductor heterojunctions [5–8,10–13,15]. In these calculations, the band structures of the interface components are aligned through a reference potential (e.g., a core level or the electrostatic potential), which is derived from a self-consistent calculation of the interface. However, semilocal DFT has the tendency to underestimate the band gap. For example, semilocal DFT gives a band gap of  $\sim 0.6$  eV for Si, which is underestimated by 50% compared to the experimental gap of 1.2 eV. Even worse, for a semiconductor like germanium, this level of theory predicts a vanishing band gap. For insulators with larger band gaps such as LiF, the band gap can be too small by over 5 eV.

Since band offsets intimately relate to band-edge positions, it is conceivable that the band offsets might also be subject to the “band-gap problem.” Indeed, this deficiency of semilocal DFT for band offsets has clearly been pointed out in the case of semiconductor-insulator interfaces [16,17].

Several schemes have been proposed for a more realistic band-gap prediction. The band-gap deficiency of (semi)local DFT has been shown to be a consequence of the delocalization error, or equivalently of the self-interaction error [18]. A mixture of Fock and semilocal exchange as in hybrid density functionals alleviates the delocalization error [19]. Furthermore, hybrid functionals are capable of reproducing the experimental band gap by optimizing the fraction of the incorporated Fock exchange, and this could be particularly important for band-offset predictions. The good performance of hybrid functionals in describing the band offsets has been demonstrated for various semiconductor heterojunctions and semiconductor-insulator interfaces [16,20].

The many-body perturbation theory within the  $GW$  approximation offers another path towards accurate determinations of the electronic band structure [21]. The  $GW$  approximation relies on a dynamic dielectric screening of the Coulomb potential and approximates the electronic self energy by a convolution in terms of the Green’s function  $G$  and the screened interaction  $W$ . The band gap is then obtained as the difference between the electron affinity and the ionization energy, which are interpreted as quasiparticle energies of the conduction-band minimum (CBM) and the valence-band maximum (VBM), respectively. In practice,  $GW$  calculations are often carried out perturbatively to correct DFT eigenvalues without further iterations, as in the one-shot  $G_0W_0$  approximation [22]. It has been shown that the one-shot  $G_0W_0$  already shows a noticeable improvement over semilocal DFT results, bringing the band gaps much closer to experimental values [23]. The quasiparticle corrections to the bulk band-edge levels are combined with the interface potential lineup evaluated at the semilocal DFT level to obtain an improved band offset. Such a  $GW$  scheme has been applied to several semiconductor-semiconductor [14,24–27] and semiconductor-oxide [17,28] heterojunctions.

<sup>\*</sup>Corresponding author: [wei.chen@epfl.ch](mailto:wei.chen@epfl.ch)

Band-offset calculations rely on two ingredients: the band structure of the individual bulk materials and the potential lineup at the interface. The improved band offsets achieved in hybrid-functional and  $GW$  calculations are however mostly credited to the more realistic band gaps [16,17]. As such, the role of band-edge positions is critical in band-offset predictions [29,30]. Meanwhile, it has been established that advanced electronic-structure methods, such as hybrid functionals and the  $GW$  approximation, tend to position the band edges differently even when they give the same band gap [31]. At present, it is not clear which method yields reliable band-edge positions. Assessing the quality of band-edge positions is not a trivial task, as the energy levels in periodic bulk calculations cannot directly be compared to experimental data [29,30]. Therefore, one needs either to determine the work function through a surface calculation, or to resort to band offsets at heterojunctions. While the former approach might appear more direct, it requires a model of the surface structure and is more subject to uncontrolled surface terminations in the experiment.

In this paper, we present a first-principles study of the band offsets for a variety of lattice-matched semiconductor heterojunctions. The considered interfaces include homovalent (e.g. GaAs/AIAs and GaP/AIP) and heterovalent heterojunctions (e.g., Ge/GaAs, Si/GaP, Ge/AIAs, ZnSe/GaAs, and Ge/ZnSe). All considered interfaces are nonpolar. First, we apply a semilocal density functional and find an overall good agreement with experiment, in accord with previous studies [10,20]. We then examine how the band alignment is affected when adopting more advanced electronic-structure methods such as hybrid functionals and  $G_0W_0$ , which generally provide an improved description of the semiconductor band gaps. In particular, we also investigate to what extent the interface dipole is affected.

The present paper is organized as follows. In Sec. II, we describe the method adopted for the band-offset determination and give the computational details of the hybrid-functional and  $G_0W_0$  calculations. In Sec. III, we calculate the band gaps and the band-edge positions of the bulk semiconductors within the various schemes. Section IV is devoted to the band offsets of the considered heterojunctions as calculated with the various electronic structure methods. In Sec. V, we specifically focus on interface dipoles by studying their variation with the fraction of Fock exchange in the hybrid functional. The conclusions are drawn in Sec. VI.

## II. METHODS

The band offsets are determined through the scheme proposed by Van de Walle and Martin [10] and Baldereschi *et al.* [12]. The valence-band offset (VBO) of a heterojunction  $A/B$  is expressed as

$$\text{VBO} = \Delta E_{\text{VBM}}^{(B-A)} + \Delta V^{(B-A)}. \quad (1)$$

The first term,  $\Delta E_{\text{VBM}}$ , is the bulk contribution which is obtained through two separate calculations of the individual bulk semiconductors  $A$  and  $B$ . The VBM of each material is referenced to a local reference potential, which corresponds to the sum of the electrostatic potential and the local pseudopotential. The interface lineup,  $\Delta V$ , is derived from the

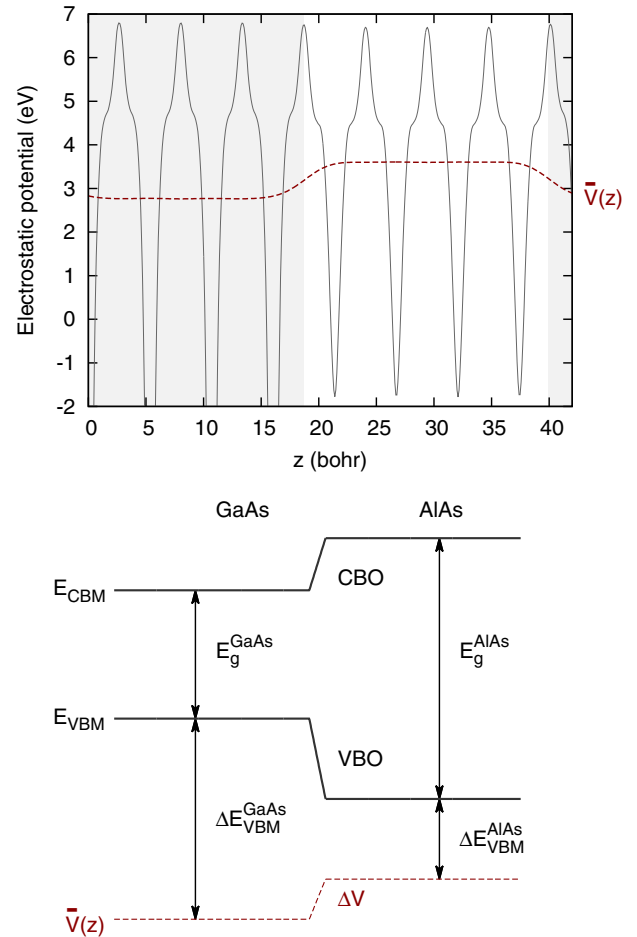


FIG. 1. (Color online) The profile of the local reference potential of the AlAs/GaAs heterojunction calculated at the PBE level along the (100) direction. The red dashed line shows the macroscopic average of the local reference potential. The calculation scheme of the VBO is illustrated in the bottom panel.

macroscopic average  $\bar{V}(z)$  of the planar average of the local reference potential  $V(z)$  along the growth direction  $z$ ,

$$\bar{V}(z) = \frac{1}{a} \int V(z-z')\theta(z')dz', \quad (2)$$

where  $a$  is the lattice constant, and  $\theta(z')$  is a unit step function defined as 1 when  $-a/2 \leq z' \leq a/2$ , and as 0 elsewhere. The convolution can be efficiently evaluated in Fourier space. A diagram depicting the lineup of the local reference potential at the interface of AlAs/GaAs is shown in Fig. 1. The conduction-band offset (CBO) can then be obtained by considering the band gaps of the two interface components (cf. Fig. 1).

In the present paper, we collect seven nonpolar interfaces with experimental VBOs ranging from 0.5 to 1.5 eV. Two interfaces show a (100) orientation, namely AlAs/GaAs and AlP/GaP. For each interface component we use four atomic layers, giving a total of 16 atoms in the tetragonal superlattice. The growth direction is (110) for the other five interfaces, i.e., Ge/GaAs, Si/GaP, Ge/AIAs, ZnSe/GaAs, and ZnSe/Ge. For these interface components, we use seven atomic layers with a total of 28 atoms in the orthorhombic superlattice. These widths ensure converged potential lineups at the

TABLE I. Variations of the potential lineup  $\delta(\Delta V^{B-A})$  (in eV) at the heterojunction interfaces  $A/B$  due to the structural relaxations, as referred to the unrelaxed case. The results are obtained at both fixed and relaxed cell parameter  $L_z$  along the  $z$  direction.

Interface $A/B$	Orientation	$\delta(\Delta V^{B-A})$	
		Fixed $L_z$	Relaxed $L_z$
AlAs/GaAs	(100)	0.00	-0.00
AlP/GaP	(100)	-0.03	-0.04
Ge/GaAs	(110)	-0.08	0.07
Si/GaP	(110)	0.08	0.01
Ge/AlAs	(110)	-0.01	0.04
ZnSe/GaAs	(110)	0.06	-0.12
Ge/ZnSe	(110)	-0.12	0.13

interfaces [32]. We denote the heterojunctions by  $A/B$  when  $A$  is epitaxially grown on top of the substrate  $B$ . To mimic the epitaxial growth condition, the lattice constant of  $A$  is therefore adapted to that of  $B$ . Throughout this paper, we use experimental lattice parameters. The choice of experimental rather than theoretical lattice parameters does not affect the final VBOs by more than 0.1 eV. We further note that structural relaxation of the interfacial atomic positions has a limited effect on the VBOs, as demonstrated in Table I. We consider two schemes of the atomic relaxation. In the first scheme the cell parameter in the growth direction ( $z$ ) is kept fixed, whereas it is allowed to fully relax in the second scheme. The changes in the potential lineup in either case are found to be negligible, within the order of 0.1 eV. This limited effect of structural relaxation is in accord with earlier studies [15,33,34]. For simplicity, all atoms in this study are thus kept at their ideal bulk positions in the interface calculations. Moreover, we do not take into account distortions resulting from the Poisson ratio as such effects are found to be very small for the mismatches in the present set of heterojunctions (below 0.4%). Spin-orbit splittings are not considered here. Estimating their effect on the VBM shift through experimental values [10], we find that the VBOs are affected by 0.03 eV or less.

The bulk calculations of every compound are performed with an  $8 \times 8 \times 8$   $\mathbf{k}$ -point mesh. The semilocal DFT calculations are based on the Perdew-Burke-Ernzerhof (PBE) exchange-correlation functional [35]. For the hybrid functional calculations, we adopt the PBE0 functional in which a fraction  $\alpha$  of PBE exchange is substituted by nonlocal Fock exchange [36]. We generally use the default value  $\alpha = 0.25$  [36]. However, to overcome issues related to different band gaps in some comparisons, we additionally also consider PBE0 calculations with  $\alpha$  scaled to match either the experimental or the  $G_0W_0$  band gap. The divergence appearing in the Fock exchange is treated with the Gygi-Baldereschi auxiliary function technique [37,38]. The semilocal and hybrid functional calculations are achieved with the QUANTUM-ESPRESSO package [39].

The  $G_0W_0$  quasiparticle corrections to the band edges use the PBE eigenfunctions and eigenvalues as the starting point. The dynamical dielectric function  $\varepsilon^{-1}(\omega)$  is obtained with a constant cutoff of 30 Ry, and is approximated by the Godby-Needs plasmon-pole model [40]. In the Godby-Needs model,

TABLE II. The numerical parameters of the  $G_0W_0$  calculations:  $\mathbf{k}$ -point sampling, ground-state cut-off energy  $E_{\text{cut}}$  (in Ry), number of (occupied and unoccupied) bands  $n_{\text{band}}$  used for the dielectric matrix and the Green's function, cut-off energy  $E_{\text{cut}}^{\text{eps}}$  (in Ry) used for the dielectric matrix.

	$\mathbf{k}$ -points	$E_{\text{cut}}$	$n_{\text{band}}$	$E_{\text{cut}}^{\text{eps}}$
Si	$8 \times 8 \times 8$	80	500	30
Ge	$8 \times 8 \times 8$	330	700	30
$zb$ -GaAs	$8 \times 8 \times 8$	330	700	30
$zb$ -AlAs	$8 \times 8 \times 8$	190	700	30
$zb$ -AlP	$8 \times 8 \times 8$	190	700	30
$zb$ -GaP	$8 \times 8 \times 8$	330	700	30
$zb$ -ZnSe	$8 \times 8 \times 8$	330	1000	30

$\varepsilon^{-1}(\omega)$  is explicitly evaluated at two points, one at the static limit ( $\omega = 0$ ) and the other at the imaginary plasmon frequency  $i\omega_p$ . Such a simple model has shown appreciable accuracy with respect to full-frequency treatments for states close to the band edges [17,31,41]. For the semiconductors considered here, we establish that the Godby-Needs model reproduces the band-edge shifts obtained with the contour deformation technique with errors smaller than 0.05 eV. Moreover, these errors tend to cancel out as far as the band offsets are concerned, as the deviations from the full frequency treatment appear to be systematic throughout the class of semiconductors considered here. In the  $G_0W_0$  calculations, we use up to 1000 bands for the evaluation of the dielectric function and the self energy. The numerical parameters adopted in the  $G_0W_0$  calculations are summarized in Table II. As in the hybrid-functional calculations, the singularity due to Fock exchange is treated with the auxiliary function approach of Gygi and Baldereschi [37]. The  $G_0W_0$  calculations are performed with the ABINIT package [42].

To calculate the interface lineups, we use an  $8 \times 8 \times 1$   $\mathbf{k}$ -point mesh. In addition to PBE, we also employ the PBE0 functional to study the effect of nonlocal Fock exchange on the interface dipole. In the evaluation of the Fock exchange energy, we find that a  $4 \times 4 \times 1$   $\mathbf{q}$ -point mesh is sufficient.

All calculations in this paper are based on norm-conserving pseudopotentials (NCPPs). The reference configurations, cut-off radii, and kinetic energy cutoffs of the NCPPs are listed in Table III. To reach a high accuracy in the  $GW$  calculations, these NCPPs are carefully constructed to reproduce the

TABLE III. The parameters of the pseudopotentials: valence electrons, cutoff radius  $r_{\text{cut}}$ , and energy cutoff  $E_{\text{cut}}$ .

	Valence	$r_{\text{cut}}$	$E_{\text{cut}}$
Al	$2s^2 2p^6 3s^2 3p^1$	0.97	190
Si	$3s^2 3p^2 3d^0$	1.95, 2.05, 1.95	60
P	$3s^2 3p^3 3d^0$	1.40, 1.45, 1.40	70
Zn	$3s^2 3p^6 3d^{10} 4s^2 4p^0$	0.80	330
Ga	$3s^2 3p^6 3d^{10} 4s^2 4p^1$	0.80	330
Ge	$3s^2 3p^6 3d^{10} 4s^2 4p^2$	0.80	330
As	$4s^2 4p^3 4d^0$	1.95, 1.75, 2.05	50
Se	$4s^2 4p^4$	1.82, 1.95	80

scattering properties up to 10 Ry above the vacuum level. Semicore states are also treated like valence electrons whenever necessary. In particular, for Zn and Ga, we include the entire third shell ( $3s$ ,  $3p$ , and  $3d$ ) among the valence electrons as these states are found essential for correctly accounting for the  $GW$  self energies [23]. For Si, the semicore states have negligible effects in  $GW$  calculations [43] and are not included here. The current treatment is designed to yield well-converged results within the framework of NCPP  $GW$  calculations. We checked that with this setup the PBE band gaps of the bulk semiconductors evaluated at their equilibrium lattice constant coincide within 0.05 eV with results obtained with projector-augmented-wave calculations reported in the literature [44,45].

### III. BAND GAPS AND BAND-EDGE SHIFTS OF BULK SEMICONDUCTORS

We first focus on the bulk semiconductors and determine the band gaps and the band-edge positions with respect to the local reference potential. The calculated band gaps are given in Table IV together with the mean absolute error (MAE) with respect to experiment. The largest deviations are observed for PBE (MAE = 0.86 eV) corresponding to band gaps underestimated by about 50% on average. An improvement is obtained for default PBE0 ( $\alpha = 0.25$ ) which leads to an overestimation of about 40% for these semiconductors.  $G_0W_0$  shows a good overall agreement with experiment (MAE = 0.15 eV), slightly underestimating the band gaps by 2% on average. We note that in Table IV three lattice constants of Ge are considered as Ge forms heterojunctions with three different substrates (GaAs, AlAs, and ZnSe). PBE tends to close the band gap of Ge at the  $\Gamma$  point regardless of the adopted lattice constant. Finite indirect  $\Gamma - L$  band gaps are recovered in PBE0 and  $G_0W_0$  (cf. Table IV).

TABLE IV. Band gaps  $E_g$  (in eV) of various semiconductors as calculated within PBE, PBE0, and  $G_0W_0$ , compared to experimental values. The calculations are performed at the experimental lattice constant  $a$  (in Å) taken from Refs. [44,46]. The mean absolute error (MAE) with respect to experiment is given (only the Ge value for  $a = 5.65$  Å is here taken into account).

	$a$	$E_g$			
		PBE	PBE0	$G_0W_0$	Expt.
Ge	5.65	0.01	1.51	0.73	0.74 <sup>a</sup>
	5.66	0.00	1.49	0.66	0.74 <sup>a</sup>
	5.67	0.00	1.46	0.63	0.74 <sup>a</sup>
Si	5.45	0.65	1.84	1.23	1.17 <sup>b</sup>
$zb$ -GaAs	5.65	0.56	2.10	1.32	1.52 <sup>b</sup>
$zb$ -AlAs	5.66	1.42	2.73	2.09	2.23 <sup>c</sup>
$zb$ -GaP	5.45	1.70	3.06	2.59	2.35 <sup>d</sup>
$zb$ -AlP	5.45	1.61	3.02	2.50	2.51 <sup>c</sup>
$zb$ -ZnSe	5.67	1.34	3.08	2.40	2.80 <sup>e</sup>
MAE		0.86	0.57	0.15	

<sup>a</sup>Photoluminescence, Ref. [47].

<sup>b</sup>Photoluminescence, Ref. [48].

<sup>c</sup>Photoluminescence, Ref. [49].

<sup>d</sup>Optical absorption, Ref. [50].

<sup>e</sup>Photoreflectance, Ref. [51].

TABLE V. Valence band-edge shifts (in eV) as obtained in PBE0 and  $G_0W_0$  for various semiconductors. The shifts are referred to the VBM obtained in the PBE, after aligning the band structures at different levels of theory through the average electrostatic potential. In the PBE0 $_{G_0W_0}$  scheme, the fraction  $\alpha$  of Fock exchange is scaled to reproduce the  $G_0W_0$  band gap. The Ge semiconductor is considered with three different lattice constants  $a$  as it matches GaAs, AlAs, and ZnSe substrates.

	PBE0	$G_0W_0$	PBE0 $_{G_0W_0}$
Ge ( $a = 5.65$ Å)	-0.71	-0.74	-0.30
Ge ( $a = 5.66$ Å)	-0.70	-0.69	-0.27
Ge ( $a = 5.67$ Å)	-0.70	-0.68	-0.27
Si	-0.67	-0.66	-0.32
$zb$ -GaAs	-0.75	-0.68	-0.38
$zb$ -AlAs	-0.79	-0.76	-0.40
$zb$ -GaP	-0.83	-0.88	-0.54
$zb$ -AlP	-0.86	-0.92	-0.55
$zb$ -ZnSe	-0.98	-0.93	-0.59

We then turn to the valence band-edge positions as obtained in PBE0 and  $G_0W_0$ , and reference them to their position in PBE (cf. Table V). In particular, Fig. 2 offers a graphical comparison between the band edges in  $G_0W_0$ , the band edges in PBE0 as the fraction of Fock exchange  $\alpha$  evolves between  $\alpha = 0$  (PBE) and  $\alpha = 0.25$  (default PBE0), and the experimental band gap. One notices that the band gap opening in  $G_0W_0$  is dominated by a downwards shift of the VBM, whereas more evenly balanced shifts of the VBM and CBM are found in PBE0 [31]. It is interesting to note in Fig. 2 that the VBM shifts are rather consistently described by the default PBE0 ( $\alpha = 0.25$ ) and  $G_0W_0$  calculations. However, this agreement does not transfer to the CBOs, since the calculated band gaps in these two schemes differ significantly (cf. Table IV). To overcome this difficulty, it is convenient to scale the PBE0 band gaps to the  $G_0W_0$  ones by adapting the fraction  $\alpha$ , a scheme denoted as PBE0 $_{G_0W_0}$  hereafter. The adapted values of  $\alpha$  are indicated in Fig. 2 for each of the semiconductors and are found to vary between 0.10 to 0.15. Upon such scaling, the PBE0 band edges are persistently higher than the corresponding ones in  $G_0W_0$  by 0.3 to 0.4 eV for all the semiconductors considered (cf. Table V).

### IV. BAND OFFSETS OF HETEROJUNCTIONS

We now combine the bulk band-edge positions with the interface lineup to derive the band offsets of the semiconductor heterojunctions. The interface lineups are derived from self-consistent PBE calculations of the interface models and used for all levels of theory throughout this section. In the next section, this approximation will be critically addressed. The derived valence band offsets are given in Table VI.

Most heterojunctions in our set show a type-I configuration in which the band edges of the wide-band-gap interface component straddle those of the low-band-gap one (cf. Fig. 1). In our set, only AIP/GaP shows the type-II (staggered) alignment, with the VBM of AIP lying below that of GaP [53]. As far as the relative position of the valence band edges is concerned, all electronic structure schemes considered in this paper qualitatively reproduce the experimental situation.

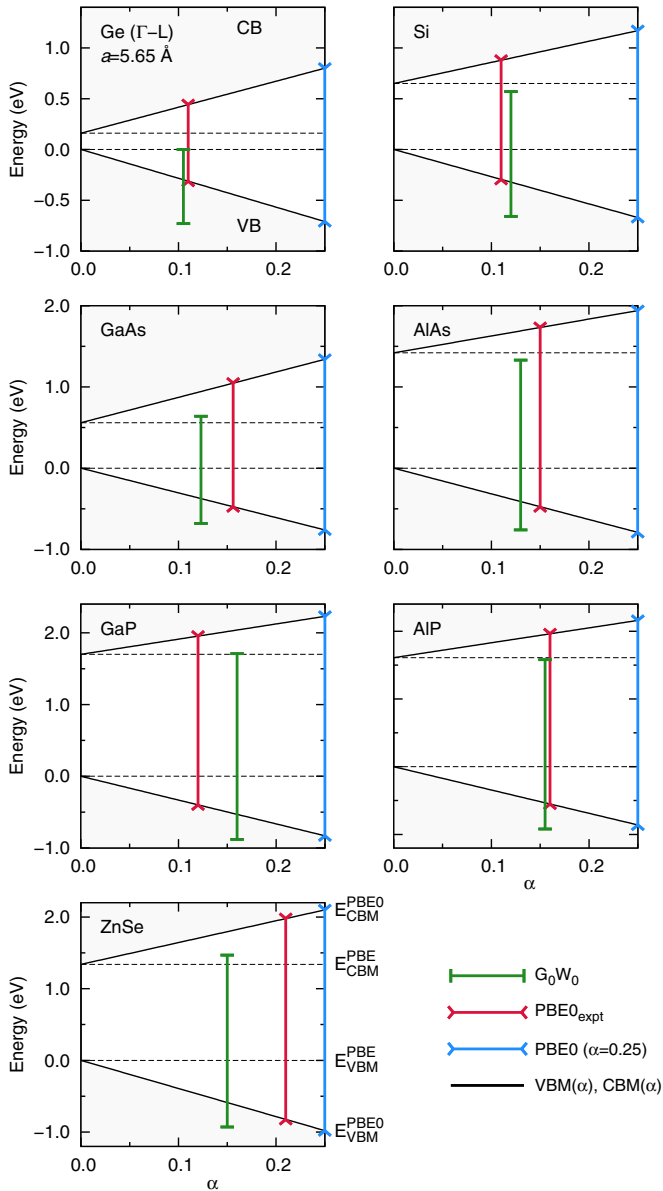


FIG. 2. (Color online) Calculated band-edge positions of the semiconductors within PBE, PBE0, and  $G_0W_0$ . The energy is referred to the VBM in the PBE and the band structures obtained within other schemes are aligned through the electrostatic potential.  $VBM(\alpha)$  and  $CBM(\alpha)$  indicate the variation of the PBE0 band-edge positions with the fraction of Fock exchange  $\alpha$ . The bar denoted  $PBE0(\alpha = 0.25)$  indicates the position of the PBE0 band gap at the default value of  $\alpha$ . The bar identified by  $PBE0_{\text{expt}}$  indicates the value of  $\alpha$  needed to reproduce the experimental band gap in PBE0. The bar denoted  $G_0W_0$  indicates the band-edge positions in  $G_0W_0$ , and is represented in correspondence of the value of  $\alpha$  for which the PBE0 band gap coincides with the  $G_0W_0$  one.

However, such a good description is not always achieved for the relative position of the conduction band edges.

As shown in Table VI, the VBOs at the PBE level of theory give a good description of the experimental data yielding a MAE of only 0.16 eV. Our results are in line with previous self-consistent PBE calculations. The VBOs of the two (100) interfaces, namely AlAs/GaAs and AlP/GaP, are consistent

TABLE VI. Valence-band offsets (in eV) at various heterojunctions as obtained from band-edge determinations in PBE, PBE0,  $G_0W_0$ ,  $PBE0_{G_0W_0}$ , compared to experimental values. The potential lineup across the interface is evaluated at the PBE level of theory. The mean absolute error (MAE) with respect to experiment is given.

	PBE	PBE0	$G_0W_0$	$PBE0_{G_0W_0}$	Expt.
AlAs/GaAs (100)	0.53	0.57	0.60	0.56	0.53 <sup>a</sup>
AlP/GaP (100)	0.64	0.68	0.67	0.64	0.55 <sup>b</sup>
Ge/GaAs (110)	0.51	0.56	0.47	0.58	0.56 <sup>c</sup>
Si/GaP (110)	0.31	0.46	0.53	0.52	0.80 <sup>d</sup>
Ge/AlAs (110)	1.07	1.15	1.14	1.20	0.95 <sup>e</sup>
ZnSe/GaAs (110)	0.89	1.11	1.13	1.11	1.10 <sup>f</sup>
Ge/ZnSe (110)	1.37	1.64	1.62	1.69	1.52 <sup>f</sup>
MAE	0.16	0.12	0.12	0.12	

<sup>a</sup>From Ref. [52] and references therein.

<sup>b</sup>From Ref. [53].

<sup>c</sup>From Ref. [54].

<sup>d</sup>From Ref. [55].

<sup>e</sup>From Ref. [56].

<sup>f</sup>From Ref. [57].

with those obtained by Van de Walle and Martin [10]. For Ge/GaAs(110), Ge/ZnSe(110), and ZnSe/GaAs(110), the VBOs compare favorably with those by Christensen [32] and Qteish and Needs [58]. For Si/GaP, for which we record the largest deviation from experiment, our result agrees within 0.2 eV with previous calculations either at the same PBE level [33,59] or in the local-density approximation (LDA) [32,58]. We specifically establish that neither the choice of the lattice parameter nor the interface relaxation affect the calculated value significantly.

At the PBE0 ( $\alpha = 0.25$ ) level, a general improvement is observed which reduces the MAE from 0.16 eV found in PBE to 0.12 (cf. Table VI). Generally, the VBOs obtained in PBE0 are larger than those in PBE by only 0.05 eV. The largest improvement is achieved for the ZnSe/GaAs heterojunctions, for which the VBO moves closer to the experimental value by  $\sim 0.2$  eV. We note that the PBE0 overestimates the band gaps of the semiconductors as much as PBE underestimates them (cf. Table IV). However, these dramatic differences in the band structure are not reflected in the VBO. Indeed, the VBM of the two semiconductors involved in a heterojunction undergo nearly identical shifts in PBE0, as can be inferred from Table V. For instance, the VBMs of both GaAs and AlAs experience a downwards shift of  $\sim 0.8$  eV. Thus, the VBM shift of GaAs is effectively counterbalanced by the shift of AlAs, leaving the VBO nearly unchanged as compared with the result in PBE.

At the  $G_0W_0$  level, the band-edge corrections give rise to VBOs with a MAE of 0.12 eV, comparable with the value achieved in PBE0. This is a direct consequence of the similar VBM shifts in PBE0 and  $G_0W_0$  for the present class of semiconductors (cf. Table V). The largest difference between theory and experiment is still for Si/GaP, but the deviation is now only 0.27 eV. Among the heterojunctions considered here, previous  $G_0W_0$  calculations have only been performed for AlAs/GaAs [14], yielding a VBO of  $0.53 \pm 0.05$  eV in agreement with our result (cf. Table VI).

TABLE VII. Conduction-band offsets (in eV) as determined from band-edge positions using various schemes. Experimental values are deduced from the corresponding experimental band gaps (cf. Table IV) and the experimental VBOs (cf. Table VI). Negative values refer to a staggered type-II band alignment. The interface dipole is evaluated at the PBE level. The mean absolute error (MAE) with respect to experiment is given.

	PBE	PBE0	$G_0W_0$	PBE0 $_{G_0W_0}$	Expt.
AlAs/GaAs (100)	-0.33	0.06	0.17	0.21	0.18
AlP/GaP (100)	-0.73	-0.72	-0.76	-0.73	-0.39
Ge/GaAs (110)	-0.11	0.04	0.13	0.01	0.21
Si/GaP (110)	0.74	0.76	0.83	0.84	0.38
Ge/AlAs (110)	0.22	0.09	0.30	0.24	0.54
ZnSe/GaAs (110)	-0.07	-0.08	-0.01	0.01	0.18
Ge/ZnSe (110)	-0.15	-0.02	0.14	0.07	0.54
MAE	0.40	0.32	0.25	0.28	

In Table VII, we provide a comparison between the calculated CBOs and their experimental reference. We obtain MAEs of 0.40, 0.32, 0.25, and 0.28 eV for PBE, PBE0,  $G_0W_0$ , and PBE0 $_{G_0W_0}$ , respectively. The agreement with experiment is noticeably worse than for the VBOs in all cases. We notice a slight decrease of the MAE as the band gap description is improved (cf. Table IV).

To assess the quality of the band alignment, it is convenient to have a theoretical description with equal band gaps in each of the interface components, thus leading to identical errors for the VBO and the CBO. For this purpose, we take advantage of the possibility of scaling the band gap in PBE0 calculations by adapting the fraction  $\alpha$  of Fock exchange.

We first compare scaled hybrid-functional to  $G_0W_0$  results. For each bulk component, we determine the fraction  $\alpha$  which ensures that the PBE0 calculation yields the same band gap as  $G_0W_0$  on either side of the heterojunction. We denote this scheme as PBE0 $_{G_0W_0}$ . As can be seen from Tables VI and VII, the PBE0 $_{G_0W_0}$  scheme produces band edges which are aligned to the  $G_0W_0$  within 0.1 eV. The MAEs with respect to experiment are also very similar in the two schemes. This result demonstrates that hybrid functionals and  $G_0W_0$  give consistent band alignments for the considered class of semiconductor heterojunctions.

Next, we are interested in estimating the accuracy of band offsets achieved within a theoretical scheme which does not suffer at all from the band gap problem. In other words, we would like to estimate the band offsets taking advantage of knowing the experimental band gaps of the interface components. Such a scheme would produce the same MAEs for VBOs and CBOs. A trivial scheme consists of relying on the calculated VBOs and to infer the associated CBOs through consideration of the experimental band gap. This approach results in the MAEs given in Table VI. In particular, for PBE0, the achieved MAE is 0.12 eV. An alternative scheme consists in scaling the fraction  $\alpha$  of Fock exchange in the hybrid functional for each interface component until the experimental band gap is recovered. This scheme, here denoted PBE0 $_{\text{expt}}$ , produced excellent band alignments for semiconductor-oxide interfaces [16]. The comparison between

TABLE VIII. Valence-band offsets (in eV) calculated in the PBE0 and compared to experimental values for various semiconductor heterojunctions. In the PBE0 calculations, the fraction  $\alpha$  of Fock exchange is adapted to match the experimental band gap of the bulk components. The interface dipole is either obtained in the PBE (PBE0 $_{\text{expt}}$ ) or in a PBE0 calculation with the fraction  $\alpha_0$  (PBE0 $_{\text{expt}}^{\alpha_0}$ ).

		PBE0 $_{\text{expt}}$	PBE0 $_{\text{expt}}^{\alpha_0}$	Expt.
AlAs/GaAs (100)	(100)	0.55	0.58	0.53
AlP/GaP (100)	(100)	0.79	0.83	0.55
Ge/GaAs (110)	(110)	0.67	0.63	0.57
Si/GaP (110)	(110)	0.41	0.37	0.80
Ge/AlAs (110)	(110)	1.24	1.24	0.95
ZnSe/GaAs (110)	(110)	1.21	1.24	1.10
Ge/ZnSe (110)	(110)	1.86	1.83	1.52
MAE		0.21	0.22	

PBE0 $_{\text{expt}}$  and experiment is given in Table VIII and results in a MAE of 0.21 eV. For the semiconductor heterojunctions studied here, the PBE0 $_{\text{expt}}$  is thus less effective in describing the band alignment than a scheme based on the calculated VBOs (cf. Table VI).

For most of the interfaces, the agreement between theoretical and experimental VBOs is generally very good. However, in the case of Si/GaP(110) and Ge/AlAs(110), the deviation from experiment is quite sizable in the PBE and persists when moving to hybrid-functional and  $G_0W_0$  schemes. As seen in Sec. II, atomic relaxations at the interface cannot be responsible for these discrepancies as the effect on the potential lineup is found to be small (cf. Table I). A possible cause for these discrepancies might come from atomic interdiffusion leading to structural reconstruction at the interface [15]. To examine this possibility, we investigate the charge transfer at our abrupt interfaces, since a large dipole density is expected to drive such reconstructions [15]. In Fig. 3(a), we show the macroscopic average of the total charge density  $\bar{\rho}$  for the Si/GaP heterojunction along the (110) direction. The charge transfer from the Si to the GaP takes place in the immediate vicinity of the interface and gives rise to a dipole density  $P$ , calculated as

$$P = \int z\bar{\rho}(z)dz. \quad (3)$$

In Fig. 3(b), the error in the VBO as obtained within the  $G_0W_0$  scheme is plotted against the interface dipole density  $P$ . It is evident that the error in the  $G_0W_0$  VBO closely correlates with  $P$ . In particular, the Si/GaP(110) and Ge/AlAs(110) interfaces exhibit the largest dipole density. This result indicates that the reduction of  $P$  would lead to a better agreement with experiment for these heterojunctions, suggesting that interdiffusion might play an important role in reducing the interface dipole and thereby affecting the band alignment. The effect of atomic interdiffusion has been shown to affect the VBO remarkably [15,60,61]. In particular, for Si/GaP(110), Lazzouni *et al.* assigned the main cause of inconsistency between the theoretical and experimental VBOs to atomic interdiffusion across the interface [33]. However, predicting the actual compositional profile and thus the associated VBO is presently beyond the possibility of

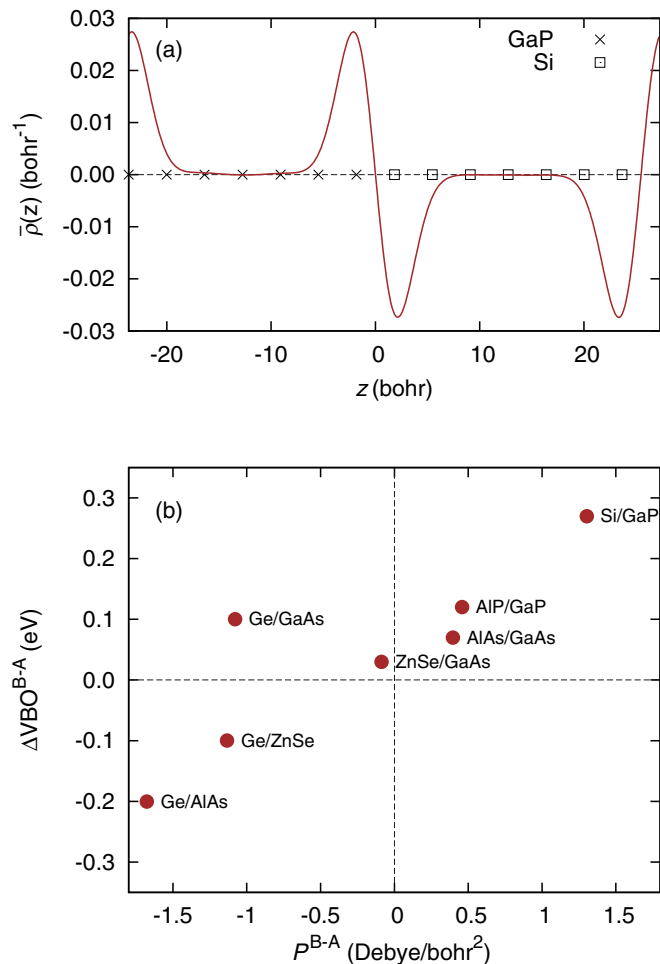


FIG. 3. (Color online) (a) Macroscopic total (electronic and ionic) charge density  $\bar{\rho}(z)$  of the Si/GaP heterojunction along the (110) direction. The positions of the atomic layers are indicated. (b) Errors in the  $G_0W_0$  VBO with respect to experiment ( $\Delta VBO^{B-A}$ ) vs the dipole density ( $P^{B-A}$ ) calculated from the macroscopic total charge density.

current computational approaches [15]. Additional difficulties in comparing theoretical and experimental VBOs might also come from the presence of defect overlayers at the interface, as suggested by List and Spicer in the case of Si/GaP(110) heterojunctions [62].

### V. EFFECT OF INTERFACE DIPOLE

In the previous section, it is assumed that the PBE is a good approximation to determine the interface potential lineup. Earlier studies on semiconductor-oxide interfaces indeed demonstrate that the PBE lineup is adequate for both hybrid-functional [16,63] and  $GW$  [17] calculations. For lattice-matched semiconductor heterojunctions, the quality of the PBE lineup has not been assessed. To this end, it is necessary to examine the interface dipole using methods going beyond semilocal density functional schemes.

Here we resort to the PBE0 hybrid functional and check how the electron density varies at the interface between the PBE and PBE0 calculations. To determine the change in the

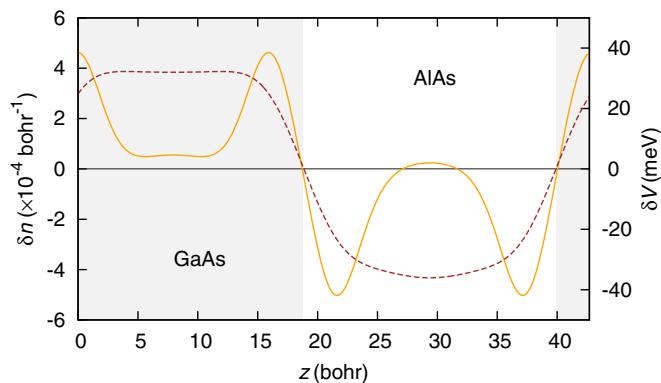


FIG. 4. (Color online) Macroscopic averages of the difference of the electron density  $\delta n$  (solid line) and of the local reference potentials  $\delta V$  (dashed line) between PBE0 ( $\alpha = 0.25$ ) and PBE calculations of the AlAs/GaAs heterojunction along the (100) direction.

lineup of the reference potential across the interface, we adopt a softer set of NCPPs for Ga, Ge, and Zn. The  $3s$  and  $3p$  electrons are removed from the valence, while the  $3d$  electrons are still retained. The soft NCPPs significantly accelerate the PBE0 calculations without compromising the determination of the interface-dipole variations.

In Fig. 4, the macroscopic average of the electron-density difference between PBE0 ( $\alpha = 0.25$ ) and PBE is displayed for AlAs/GaAs along the (100) direction. At the interface, PBE0 induces a small additional charge transfer ( $\sim 0.001e$ ) from AlAs to GaAs, thereby slightly modifying the interface dipole achieved in the PBE. This extra interface dipole lifts (lowers) the local reference potential of GaAs (AlAs) by 30 meV. As a result, the interface lineup  $\Delta V$  is decreased by 60 meV (cf. Fig. 1). For all the semiconductor heterojunctions studied here, we recorded a similarly small variation in the interface lineup.

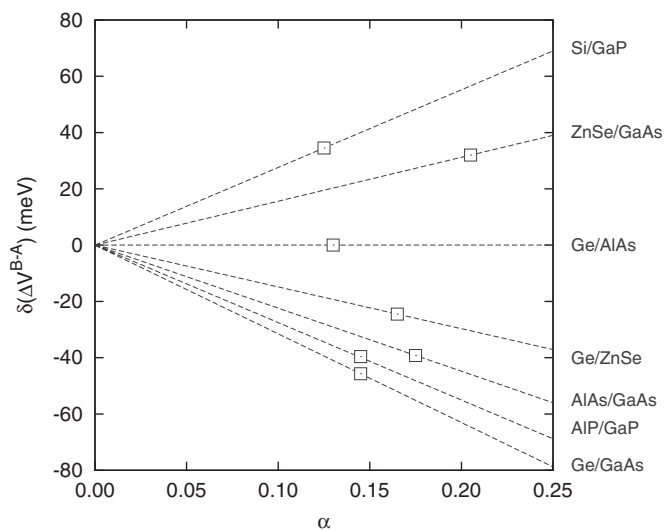


FIG. 5. Electrostatic-potential lineup  $\Delta V^{B-A}$  of various heterostructure  $A/B$  evaluated as a function of the fraction of Fock exchange  $\alpha$  in PBE0 and expressed with respect to the lineup in PBE. The open squares denote the values of  $\alpha_0$  for the considered interfaces.

As shown in Fig. 5, the use of PBE0 (for any  $\alpha \leq 0.25$ ) affects the interface lineup by no more than 80 meV. Hence, we note that the large shifts of the bands induced in PBE0 do not imply any significant effect on the potential lineup at the interface.

Next, we evaluate whether these small variations in the lineup of the local reference potential actually lead to an improvement of the valence-band offset obtained with the PBE lineup. The choice of the fraction of Fock exchange  $\alpha$  to be used in the interface calculation is not trivial as the optimal  $\alpha$  required to reproduce the experimental band gap varies from one semiconductor to another (cf. Fig. 2). We here follow the strategy described in Ref. [16]. First, we determine the optimal fraction of Fock exchange  $\alpha_A$  and  $\alpha_B$  for each of the bulk components  $A$  and  $B$ , respectively. The band edges of each component are aligned with respect to the respective local reference potential using the material-specific  $\alpha$ . Then the interface calculation is carried out using the average of  $\alpha_A$  and  $\alpha_B$ ,  $\alpha_0 = (\alpha_A + \alpha_B)/2$ . Accordingly, the VBO is obtained through the interface line-up calculated with  $\alpha_0$ . This scheme is identical to the PBE0<sub>expt</sub> introduced in Sec. IV, except for the use of  $\alpha = \alpha_0$  rather than  $\alpha = 0$  (i.e., PBE) in the interface calculations. As highlighted in Fig. 5, variations in the lineup of the local reference potential due to the use of  $\alpha_0$  give changes of  $\sim 40$  meV. These small interface lineup variations do not yield any noticeable change in the calculated VBOs as compared to the use of PBE lineups (cf. Table VIII).

Note that the perturbative  $G_0W_0$  approach does not imply any change of the interface dipole as the charge density is not updated. In Ref. [17], a  $GW$  scheme in which the electron density was self-consistently evolved was applied to a semiconductor-oxide interface. The lineup variation was found to remain unchanged with respect to the PBE within 20 meV. This result further confirms the notion that the interface dipole is already well accounted for in PBE.

## VI. DISCUSSION AND CONCLUSION

In the present paper, we employ the semilocal functional PBE, the hybrid functional PBE0, and the perturbative  $G_0W_0$  approximation to calculate the band offsets of a series of lattice-matched semiconductor heterojunctions. In the adopted PBE0 and  $G_0W_0$  schemes, we correct the band-edge positions of the bulk components without modifying the interface lineup obtained at the PBE level. We find that the lineups of the local reference potentials obtained in PBE barely change when using the more advanced PBE0 scheme, in accord with previous findings for semiconductor-insulator interfaces [16,17].

Despite its inherent band-gap problem, PBE is found to be adequate for describing the VBOs of these semiconductor heterojunctions, as generally recognized in the literature [10]. At variance, the underestimation of the band gap leads to significant errors on the CBOs. The use of the PBE0 and  $G_0W_0$  schemes improves both the VBOs and the CBOs. However, the improvement of the VBOs is strikingly small and contrasts with the significant band gap openings achieved. Inspection of the corrected valence-band edges shows that the same shifts are achieved throughout the class of considered semiconductors for either PBE0 or  $G_0W_0$ . The profound reason for this behavior cannot trivially be inferred from our calculations, but this property clearly lies at the origin of the success of (semi)local functionals in predicting VBOs for semiconductor heterojunctions [10]. It should be understood that this property does not hold for any material. For instance, insulators generally yield larger shifts than semiconductors [31]. Indeed, the VBOs at semiconductor-insulator interfaces cannot reliably be obtained at the semilocal level [16,17,63].

One important finding in this paper is that hybrid functionals and  $G_0W_0$  calculations yield a consistent description of the band alignment for this class of heterojunctions. The consistency can be inferred in two different ways. First, the VBOs achieved in default PBE0 and  $G_0W_0$  differ by less than 0.1 eV. Second, when employing hybrid functionals which yield identical band gaps as  $G_0W_0$ , the largest difference is found to be 0.12 eV. The overall consistency between hybrid functionals and  $G_0W_0$  prevents us from determining which electronic-structure method yields more accurate band-edge positions from the present heterojunctions [64,65].

Our paper also discusses the best way of taking advantage of available experimental band gaps in evaluating band offsets. For the present heterojunctions, the calculated VBOs in the default schemes enable the most accurate determination of the band alignment (MAE = 0.12 eV). An alternative scheme based on hybrid functionals designed to match the experimental band gaps yields slightly larger errors (MAE = 0.21 eV) but carries the potential of being transferable to a larger class of interfaces [16].

## ACKNOWLEDGMENTS

We acknowledge fruitful discussions with A. Baldereschi and M. Peressi. This paper is partially supported by the Swiss National Science Foundation (Grant No. 200020-134600). We used computational resources of CSEA-EPFL and CSCS.

---

[1] A. Franciosi and C. G. Van de Walle, *Surf. Sci. Rep.* **25**, 1 (1996).  
 [2] R. Anderson, *Solid State Electron.* **5**, 341 (1962).  
 [3] W. R. Frensley and H. Kroemer, *Phys. Rev. B* **16**, 2642 (1977).  
 [4] C. Tejedor and F. Flores, *J. Phys. C: Solid State* **11**, L19 (1978).  
 [5] W. E. Pickett, S. G. Louie, and M. L. Cohen, *Phys. Rev. B* **17**, 815 (1978); **18**, 2966 (1978).  
 [6] W. E. Pickett and M. L. Cohen, *Phys. Rev. B* **18**, 939 (1978).  
 [7] J. Ihm and M. L. Cohen, *Phys. Rev. B* **20**, 729 (1979).

[8] K. Kunc and R. M. Martin, *Phys. Rev. B* **24**, 3445 (1981).  
 [9] J. Tersoff, *Phys. Rev. B* **30**, 4874 (1984).  
 [10] C. G. Van de Walle and R. M. Martin, *J. Vac. Sci. Technol., B* **4**, 1055 (1986); *Phys. Rev. B* **35**, 8154 (1987).  
 [11] S.-H. Wei and A. Zunger, *Phys. Rev. Lett.* **59**, 144 (1987).  
 [12] A. Baldereschi, S. Baroni, and R. Resta, *Phys. Rev. Lett.* **61**, 734 (1988).  
 [13] S. Massidda, B. Min, and A. Freeman, *Superlattice Microst.* **4**, 15 (1988).

- [14] S. Zhang, D. Tomnek, S. G. Louie, M. L. Cohen, and M. S. Hybertsen, *Solid State Commun.* **66**, 585 (1988); S. B. Zhang, M. L. Cohen, S. G. Louie, D. Tománek, and M. S. Hybertsen, *Phys. Rev. B* **41**, 10058 (1990).
- [15] M. Peressi, N. Binggeli, and A. Baldereschi, *J. Phys. D: Appl. Phys.* **31**, 1273 (1998).
- [16] A. Alkauskas, P. Broqvist, F. Devynck, and A. Pasquarello, *Phys. Rev. Lett.* **101**, 106802 (2008).
- [17] R. Shaltaf, G.-M. Rignanese, X. Gonze, F. Giustino, and A. Pasquarello, *Phys. Rev. Lett.* **100**, 186401 (2008).
- [18] P. Mori-Sánchez, A. J. Cohen, and W. Yang, *Phys. Rev. Lett.* **100**, 146401 (2008).
- [19] A. D. Becke, *J. Chem. Phys.* **98**, 1372 (1993).
- [20] A. Wadehra, J. W. Nicklas, and J. W. Wilkins, *Appl. Phys. Lett.* **97**, 092119 (2010).
- [21] L. Hedin, *Phys. Rev.* **139**, A796 (1965).
- [22] M. S. Hybertsen and S. G. Louie, *Phys. Rev. B* **34**, 5390 (1986).
- [23] M. Shishkin and G. Kresse, *Phys. Rev. B* **74**, 035101 (2006).
- [24] D. Cociorva, W. G. Aulbur, and J. W. Wilkins, *Solid State Commun.* **124**, 63 (2002).
- [25] C. Mietze, M. Landmann, E. Rauls, H. Machhadani, S. Sakr, M. Tchernycheva, F. H. Julien, W. G. Schmidt, K. Lischka, and D. J. As, *Phys. Rev. B* **83**, 195301 (2011).
- [26] C. Mitra, B. Lange, C. Freysoldt, and J. Neugebauer, *Phys. Rev. B* **84**, 193304 (2011).
- [27] A. Punya and W. R. L. Lambrecht, *Phys. Rev. B* **88**, 075302 (2013).
- [28] M. Grüning, R. Shaltaf, and G.-M. Rignanese, *Phys. Rev. B* **81**, 035330 (2010).
- [29] A. Alkauskas, P. Broqvist, and A. Pasquarello, *Phys. Stat. Solidi B* **248**, 775 (2011).
- [30] A. Alkauskas and A. Pasquarello, *Phys. Rev. B* **84**, 125206 (2011).
- [31] W. Chen and A. Pasquarello, *Phys. Rev. B* **86**, 035134 (2012); **88**, 119906(E) (2013).
- [32] N. E. Christensen, *Phys. Rev. B* **37**, 4528 (1988).
- [33] M. E. Lazzouni, M. Peressi, and A. Baldereschi, *Appl. Phys. Lett.* **68**, 75 (1996).
- [34] M. Peressi, F. Favot, and A. Baldereschi, in *Conference Proceedings on Advances in Computational Material Science I*, Vol. 55, edited by V. Fiorentini and F. Meloni (SIF, Bologna, 1997), p. 13.
- [35] J. P. Perdew, K. Burke, and M. Ernzerhof, *Phys. Rev. Lett.* **77**, 3865 (1996).
- [36] J. P. Perdew, M. Ernzerhof, and K. Burke, *J. Chem. Phys.* **105**, 9982 (1996).
- [37] F. Gygi and A. Baldereschi, *Phys. Rev. B* **34**, 4405 (1986).
- [38] P. Broqvist, A. Alkauskas, and A. Pasquarello, *Phys. Rev. B* **80**, 085114 (2009).
- [39] P. Giannozzi, S. Baroni, N. Bonini, M. Calandra, R. Car, C. Cavazzoni, D. Ceresoli, G. L. Chiarotti, M. Cococcioni, I. Dabo, A. D. Corso, S. de Gironcoli, S. Fabris, G. Fratesi, R. Gebauer, U. Gerstmann, C. Gougoussis, A. Kokalj, M. Lazzeri, L. Martin-Samos, N. Marzari, F. Mauri, R. Mazzarello, S. Paolini, A. Pasquarello, L. Paulatto, C. Sbraccia, S. Scandolo, G. Sclauzero, A. P. Seitsonen, A. Smogunov, P. Umari, and R. M. Wentzcovitch, *J. Phys.: Condens. Matter* **21**, 395502 (2009).
- [40] R. W. Godby and R. J. Needs, *Phys. Rev. Lett.* **62**, 1169 (1989).
- [41] M. Stankovski, G. Antonius, D. Waroquiers, A. Miglio, H. Dixit, K. Sankaran, M. Giantomassi, X. Gonze, M. Côté, and G.-M. Rignanese, *Phys. Rev. B* **84**, 241201 (2011).
- [42] X. Gonze, B. Amadon, P.-M. Anglade, J.-M. Beuken, F. Bottin, P. Boulanger, F. Bruneval, D. Caliste, R. Caracas, M. Côté, T. Deutsch, L. Genovese, P. Ghosez, M. Giantomassi, S. Goedecker, D. Hamann, P. Hermet, F. Jollet, G. Jomard, S. Leroux, M. Mancini, S. Mazevet, M. Oliveira, G. Onida, Y. Pouillon, T. Rangel, G.-M. Rignanese, D. Sangalli, R. Shaltaf, M. Torrent, M. Verstraete, G. Zerah, and J. Zwanziger, *Comput. Phys. Commun.* **180**, 2582 (2009).
- [43] M. L. Tiago, S. Ismail-Beigi, and S. G. Louie, *Phys. Rev. B* **69**, 125212 (2004).
- [44] L. Schimka, J. Harl, and G. Kresse, *J. Chem. Phys.* **134**, 024116 (2011).
- [45] J. L. Lyons, A. Janotti, and C. G. Van de Walle, *Appl. Phys. Lett.* **95**, 252105 (2009).
- [46] U. Hotje, C. Rose, and M. Binnewies, *Solid State Sci.* **5**, 1259 (2003).
- [47] Y. Varshni, *Physica* **34**, 149 (1967).
- [48] O. Madelung, *Semiconductors: Data Handbook*, Vol. 3 (Springer, Berlin, 2004).
- [49] B. Monemar, *Phys. Rev. B* **8**, 5711 (1973).
- [50] R. G. Humphreys, U. Rössler, and M. Cardona, *Phys. Rev. B* **18**, 5590 (1978).
- [51] R. H. Bube, *Phys. Rev.* **98**, 431 (1955).
- [52] I. Vurgaftman, J. R. Meyer, and L. R. Ram-Mohan, *J. Appl. Phys.* **89**, 5815 (2001).
- [53] S. Nagao, T. Fujimori, H. Gotoh, H. Fukushima, T. Takano, H. Ito, S. Koshihara, and F. Minami, *J. Appl. Phys.* **81**, 1417 (1997).
- [54] J. Waldrop, E. Kraut, S. Kowalczyk, and R. Grant, *Surf. Sci.* **132**, 513 (1983).
- [55] P. Perfetti, F. Patella, F. Sette, C. Quaresima, C. Capasso, A. Savoia, and G. Margaritondo, *Phys. Rev. B* **30**, 4533 (1984).
- [56] M. K. Kelly, D. W. Niles, E. Colavita, G. Margaritondo, and M. Henzler, *Appl. Phys. Lett.* **46**, 768 (1985).
- [57] S. P. Kowalczyk, E. A. Kraut, J. R. Waldrop, and R. W. Grant, *J. Vac. Sci. Technol.* **21**, 482 (1982).
- [58] A. Qteish and R. J. Needs, *Phys. Rev. B* **45**, 1317 (1992).
- [59] O. Romanyuk, T. Hannappel, and F. Grosse, *Phys. Rev. B* **88**, 115312 (2013).
- [60] R. G. Dandrea, S. Froyen, and A. Zunger, *Phys. Rev. B* **42**, 3213 (1990).
- [61] M. Peressi, F. Favot, G. Cangiani, and A. Baldereschi, *Appl. Phys. Lett.* **81**, 5171 (2002).
- [62] R. S. List and W. E. Spicer, *J. Vac. Sci. Technol. B* **6**, 1228 (1988).
- [63] P. Broqvist, J. F. Binder, and A. Pasquarello, *Appl. Phys. Lett.* **94**, 141911 (2009).
- [64] A. Alkauskas, P. Broqvist, and A. Pasquarello, *Phys. Rev. Lett.* **101**, 046405 (2008).
- [65] W. Chen and A. Pasquarello, *Phys. Rev. B* **88**, 115104 (2013).